PHILOSOPHICAL TRANSACTIONS OF THE ROYAL SOCIETY A

Phil. Trans. R. Soc. A (2011) **369**, 3575–3587
doi:10.1098/rsta.2011.0128

Bose–Einstein condensation of spin wave quanta at room temperature

By O. Dzyapko[1], V. E. Demidov[1], G. A. Melkov[2] and S. O. Demokritov[1,*]

[1]*Institute for Applied Physics, University of Münster, 48149 Münster, Germany*
[2]*Department of Radiophysics, National Taras Schevchenko University of Kiev, Kiev, Ukraine*

Spin waves are delocalized excitations of magnetic media that mainly determine their magnetic dynamics and thermodynamics at temperatures far below the critical one. The quantum-mechanical counterparts of spin waves are magnons, which can be considered as a gas of weakly interacting bosonic quasi-particles. Here, we discuss the room-temperature kinetics and thermodynamics of the magnon gas in yttrium iron garnet films driven by parametric microwave pumping. We show that for high enough pumping powers, the thermalization of the driven gas results in a quasi-equilibrium state described by Bose–Einstein statistics with a non-zero chemical potential. Further increases of the pumping power cause a Bose–Einstein condensation documented by an observation of the magnon accumulation at the lowest energy level. Using the sensitivity of the Brillouin light scattering spectroscopy to the degree of coherence of the scattering magnons, we confirm the spontaneous emergence of coherence of the magnons accumulated at the bottom of the spectrum, occurring if their density exceeds a critical value.

Keywords: spin waves; magnons; Bose–Einstein condensation

1. Introduction

The concept of spin waves, as the lowest lying magnetic states above the ground state of a magnetic medium, was introduced by Bloch [1]. Contrary to the Stoner excitation representing a localized reversed spin, Bloch considered an excitation consisting of many spins deviating slightly from their equilibrium orientation. These disturbances propagate as waves through the medium, forming spin waves. As the temperature increases, spins deviate more and more from the common direction, thus increasing the amplitude of spin waves and reducing the net magnetization. Based on this spin wave theory, Bloch was able to predict that the magnetization of a three-dimensional ferromagnet at low temperatures should deviate from its zero-temperature value following a $T^{3/2}$ dependence, instead of an exponential dependence predicted by mean field theory.

*Author for correspondence (demokrit@uni-muenster.de)

One contribution of 10 to a Discussion Meeting Issue ‘The spin on electronics’.

The unique properties of spin waves result from interactions acting between magnetic moments. For relatively small wavevectors ($k < 10^4\,\mathrm{cm}^{-1}$), spin wave dynamics is almost entirely determined by magnetic dipole interactions. Owing to the anisotropic nature of the magnetic dipole interactions, the frequency of a spin wave depends not only on the absolute value of its wavevector, but also on the orientation of the wavevector relative to the static magnetization. For large wavevectors ($k > 10^6\,\mathrm{cm}^{-1}$), the exchange interaction dominates. In the wavevector interval $10^4\,\mathrm{cm}^{-1} < k < 10^6\,\mathrm{cm}^{-1}$, neither of these interactions can be neglected. The corresponding excitations should be treated as dipole-exchange spin waves.

From the quantum-mechanical point of view, the spin wave energy should be quantized. The quantitative theory of quantized spin waves, or magnons, was developed by Holstein & Primakoff [2] and Dyson [3]. If one considers the completely magnetized state at zero temperature as the vacuum state of the ferromagnet, the low-temperature state can be treated as a gas of magnons. The magnons behave as weakly interacting quasi-particles obeying Bose–Einstein statistics. Magnons at thermal equilibrium do not usually show coherence effects. In fact, they form a gas of excitations, nicely described within the quantum formalism of population numbers.

One of the most striking quantum phenomena possible in a gas of bosons is Bose–Einstein condensation (BEC) [4]. It represents a formation of a collective macroscopic quantum state of bosons. As the temperature of the boson gas T decreases at a given density N, or, vice versa, the density increases at a given temperature, and the chemical potential μ, describing the gas, increases as well. On the other hand, μ cannot be larger than the minimum energy of the bosons $\varepsilon_{\min}$. The condition $\mu(N, T) = \varepsilon_{\min}$ defines a critical density $N_{\mathrm{c}}(T)$. If the density of the particles in the system is larger than N_{c}, BEC takes place and the gas is spontaneously divided into two fractions: (i) particles with the density N_{c} are distributed over the entire spectrum of possible boson states and (ii) a coherent ensemble of particles is accumulated in the lowest state with $\varepsilon = \varepsilon_{\min}$.

Several groups have reported observations of field-induced BEC of magnetic excitations in different quantum low-dimensional magnets (for a review, see [5]). In these materials, a phase transition occurs if the applied magnetic field is strong enough to overcome the antiferromagnetic exchange coupling. Such a transition is accompanied by a magnetic mode softening ($\varepsilon_{\min} \to 0$). It can be treated as BEC in an ensemble of magnetic bosons. If, however, a gap exists in the magnon spectrum ($\varepsilon_{\min} > 0$), there is no possibility of observing BEC at true thermodynamic equilibrium because $\mu < \varepsilon_{\min}$. In fact, if the magnetic subsystem stays in equilibrium with the thermal bath (lattice), its state is characterized by the minimum of the free energy, F (e.g. [6]). On the other hand, the chemical potential is the derivative of the free energy with respect to the number of particles. In a system of quasi-particles whose number can vary, F can be minimized through creation and annihilation of particles. In other words, quasi-particles will be created or annihilated owing to energy exchange with the lattice until their number corresponds to the condition of the minimum F (this is the same as $\mu = 0$). Thus, to observe BEC in a gas of quasi-particles with $\varepsilon_{\min} > 0$, one should drive the system away from the true equilibrium using an external source. In the case of polaritons, one uses a laser [7], in the case of magnons, parametric microwave pumping is a perfect tool for this purpose.

In this paper, we consider BEC in a magnon gas in yttrium iron garnet (YIG) films driven by microwave parametric pumping at room temperature. We will show that the BEC transition is revealed in the experiments as an enormous overpopulation of the lowest energy level. At the same time, the thermodynamic state of the driven gas is not evident since quasi-particles possess a finite lifetime, which is often comparable with the time needed to reach thermal equilibrium. Therefore, the kinetics of the pumped magnons and their thermalization will be discussed in detail. Moreover, BEC should be accompanied by the spontaneous emergence of coherence. We will discuss experimental findings demonstrating such emergence in the magnon gas.

2. Experimental set-up

The experimental set-up used for the studies is illustrated in figure 1. The experiments were performed on monocrystalline films of YIG with a thickness of 5 µm. YIG ($Y_3Fe_2(FeO_4)_3$) films are characterized by very small magnetic losses providing a long magnon lifetime, which appears to be much longer than the characteristic time of the magnon–magnon interaction [8]. This relation is a necessary precondition for the BEC in a gas of quasi-particles whose number is not exactly conserved [7]. Samples with lateral sizes of several millimetres were cut from the films and were placed into a uniform static magnetic field of $H = 700$–1000 Oe oriented in the plane of the film. The injection of magnons was performed by means of parametric microwave pumping with a frequency of 8.0–8.1 GHz. The pumping field was created using a microstrip resonator with a width of 25 µm attached to the surface of the sample. The peak pumping power was varied from 0.1 to 6 W. Two types of pumping pulses were used: (i) short pumping pulses with a duration of 30 ns, which is shorter than the characteristic thermalization time in the magnon gas, and (ii) long pumping pulses of 1 µs duration. In the first case, studying the system *after* the pulse, there is a possibility to follow the dynamics of the magnon gas, which is free from any external driving force. For long pumping pulses, the magnon dynamics was investigated *during* the pulse. To avoid thermal overheating of the sample via intensive microwave radiation, pumping was performed in an intermittent pulsed mode with an on/off ratio of 1/20. Note here that different resonators were used for short-pulse and long-pulse pumping; therefore, a direct comparison of the pumping powers provided for these different experimental conditions is impossible. Moreover, the experiments with short-pumping pulses were performed at an applied magnetic field of $H = 1000$ Oe ($f_{\min} = 3.0$ GHz), whereas long-pulse-pumping studies were mainly performed at $H = 700$ Oe ($f_{\min} = 2.1$ GHz).

The redistribution of magnons over the spectrum was studied with a temporal resolution of 10 ns using time-resolved Brillouin light scattering (BLS) spectroscopy. The frequency resolution of the BLS set-up was good enough to detect changes in the magnon distribution over the spectrum. Both quasi-backward [8] and quasi-forward scattering geometries [9] were used. Applying the quasi-backward geometry, one simultaneously detects magnons from the wavevector interval $k = \pm 2 \times 10^5\,\mathrm{cm}^{-1}$ determined by the wavevector of the incident light. In this case, one loses the wavevector selectivity: the BLS intensity at a given frequency is the product of the magnon population at this

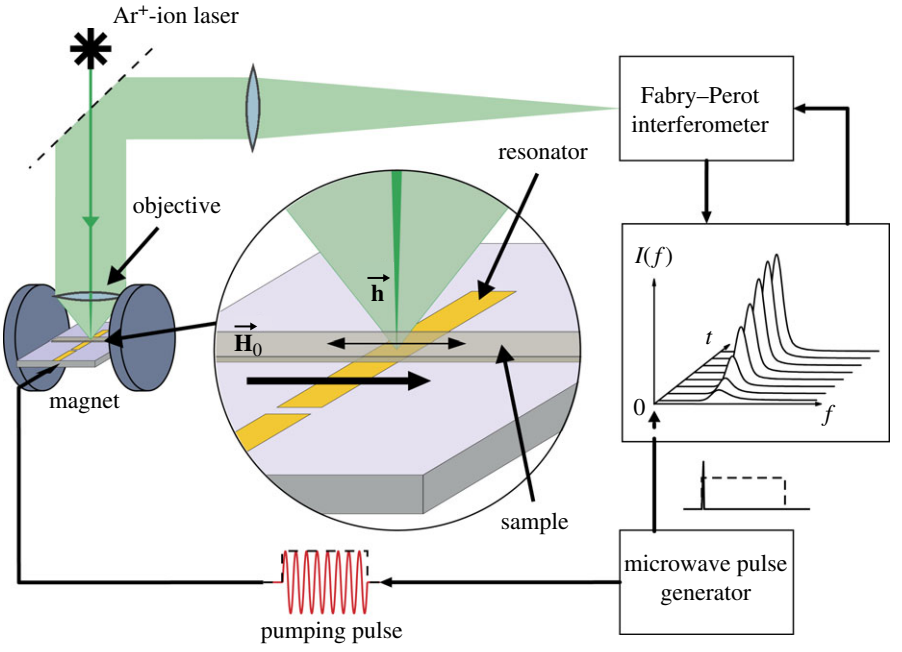

Figure 1. Experimental set-up for time-resolved investigation of redistribution over the spectrum of pumped magnons. (Online version in colour.)

frequency and the reduced magnon density of states, integrated over the above wavevector interval. Alternatively, in the quasi-forward geometry, one can record the distribution of magnons as a two-dimensional map in the wavevector space restricted by $k = \pm 5 \times 10^4\,\mathrm{cm}^{-1}$ in both in-plane directions. The experiments were performed at room temperature. A detailed description of the used BLS set-up can be found elsewhere [10,11].

Figure 2 illustrates the process of parametric pumping. It shows the low-energy part of the dispersion spectrum of magnons in an in-plane magnetized ferromagnetic film calculated for the parameters of the YIG film used and a magnetic field of $H = 700\,\mathrm{Oe}$. As mentioned above, the spectrum is anisotropic owing to the influence of the magnetic dipole interaction. The non-zero minimum frequency $f_{\min} = 2.10\,\mathrm{GHz}$ corresponds to a finite value of the wavevectors $\mathbf{k}$ oriented parallel to the static magnetic field $\mathbf{H}$, as indicated in figure 2. The frequency minimum at a non-zero wavevector results from the competition between the magnetic dipole interaction and the exchange interaction. Note, that the change of the static magnetic field H shifts $f_{\min}$, whereas by changing the film thickness, one varies the corresponding wavevector.

The process of the parametric pumping can be considered as a creation of two primary magnons by a microwave photon of the pumping field with a frequency of $2f_{\mathrm{P}}$. Owing to the energy conservation law, the frequency of primary magnons is f_{P}. Owing to the momentum conservation law, the two created magnons have opposite wavevectors. However, as seen in the figure, a manifold of magnon pairs can be excited with the allowed values of $\mathbf{k}$ building an elliptic contour on the

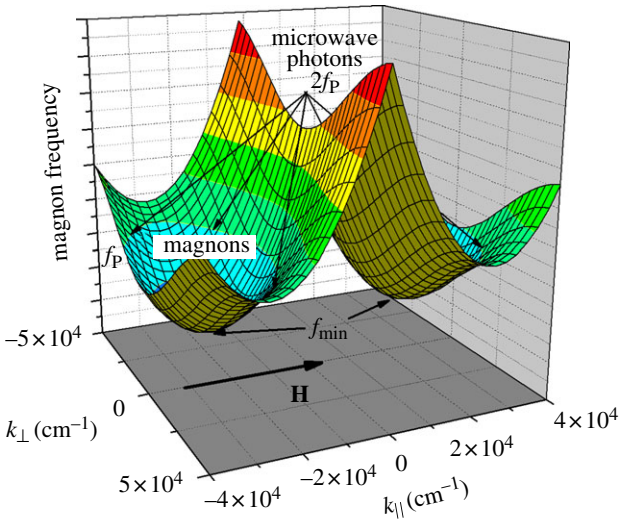

Figure 2. Calculated dispersion spectrum of magnons in an in-plane magnetized YIG film. $k_{||}$ and $k_\perp$ correspond to the components of the magnon wavevector parallel and perpendicular to the static magnetic field, respectively. The arrows illustrate the process of parametric pumping of magnons. (Online version in colour.)

($k_{||}$, $k_\perp$)-plane, where the notations $k_{||}$ and $k_\perp$ correspond to the components of the magnon wavevector parallel and perpendicular to the static magnetic field, respectively.

3. Kinetics of primary magnons and thermalization

The pumping initiates a strongly non-equilibrium magnon distribution: primary magnons with a very high density of 10^{18}–$10^{19}\,\mathrm{cm}^{-3}$ occupy the part of the spectrum close to f_P. Before considering the BEC transition caused by these additionally excited magnons, one has to clarify how they are thermalized and how a new quasi-equilibrium state of the magnon gas is created.

As mentioned above, in the quasi-forward scattering geometry, the experimental set-up enables simultaneous measurements of the wavevector of magnons and their frequency. Thus, it is very well suited to investigation of the redistribution of primary magnons after the pumping pulse. For further analysis of the magnon kinetics, we will use the representation of the magnon distribution over the spectrum in the form of colour-coded contours on the ($k_{||}$, $k_\perp$)-plane, as shown in figure 3.

Figure 3*a–f* demonstrates the magnon distribution as a two-dimensional map for different delays τ after the start of the pumping pulse, as indicated. White lines in the graphs are the contours of constant magnon frequency, whereas the white pluses indicate the point of the minimum frequency of the magnons, f_{min}. As seen from figure 3*a*, already at 20 ns after the start of the pumping pulse, the primary magnons occupy multiple states with different combinations of $k_{||}$ and $k_\perp$ lying on the contour corresponding to the constant frequency $f_P = 4.1$ GHz.

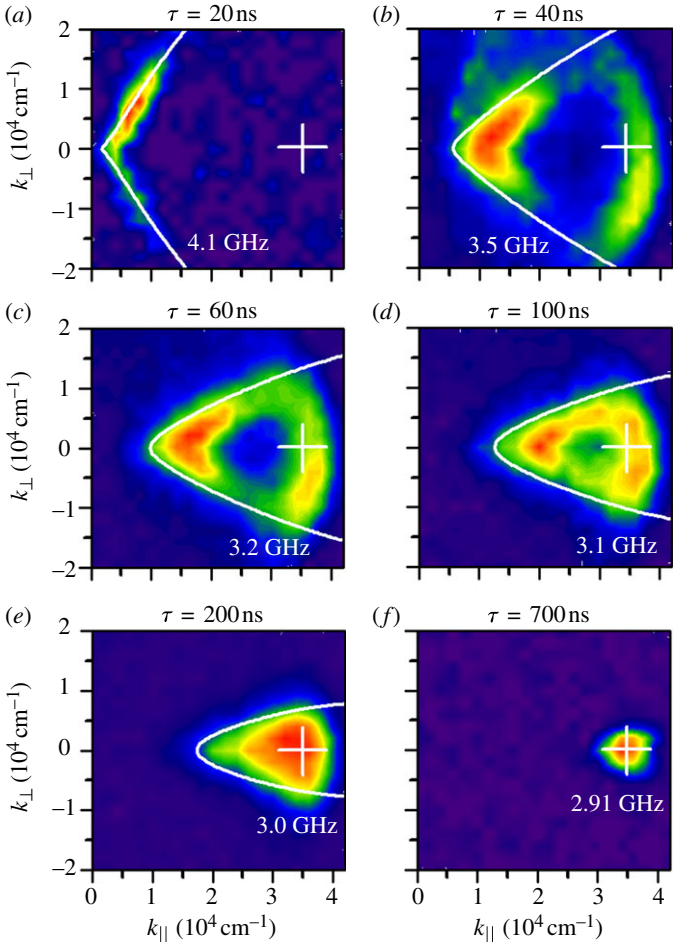

Figure 3. Colour-coded two-dimensional map of normalized BLS intensity measured for different two-dimensional magnon wavevectors $\mathbf{k}_m = (k_{||}, k_\perp)$. (*a*)–(*f*) Correspond to different delays τ after the start of the pumping pulse, as indicated. White lines are constant-frequency contours for different frequencies as indicated. The white pluses mark the position of the bottom of the magnon spectrum. $H = 1000$ Oe, $f_P = 4.1$ GHz.

The free kinetics of the pumped magnons after the pumping pulse is illustrated by figure 3*b*–*f*. The magnons redistribute over the phase space in such a way that the maximum occupation is continuously shifted with time towards the point corresponding to the bottom of the magnon spectrum. This tendency is clearly already seen at the delay $\tau = 40$ ns (figure 3*b*). Moreover, in figure 3*b*, one can also see magnons approaching the bottom of the spectrum from the exchange-dominated part of the wavevector space ($k_{||} > k_{||}^{\min}$). This fact means that the primary magnons are also created in the exchange-dominated part of the spectrum, but they are not accessible in our experiment owing to their very large wavevectors. Nevertheless, even measurements in the accessible range of 0–$4.2 \times 10^4\,\mathrm{cm}^{-1}$ allow the important conclusion that both dipole-dominated and exchange-dominated magnons contribute to the BEC. As seen from figure 3*b*–*e*,

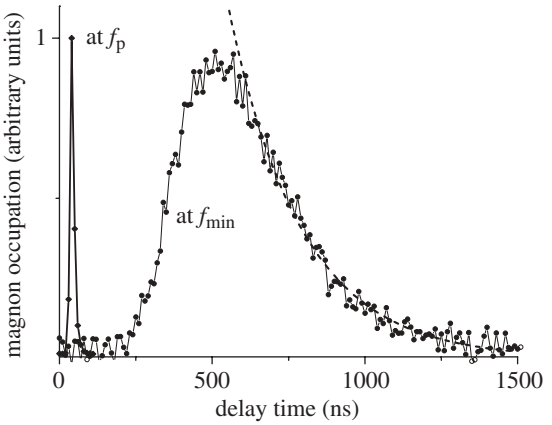

Figure 4. Magnon occupation for the primary magnons (f_P) and magnons at the minimum frequency (f_{min}) for pumping by short pulses, $P = 2$ W. Dashed line represents an exponential decay corresponding to a lifetime of 260 ns.

the kinetics of these two groups of magnons is essentially different. The dipole-dominated magnons approach the bottom of the spectrum rather slowly (150–200 ns), and in every stage are distributed along the line of equal frequency. By contrast, the exchange-dominated magnons reach the bottom of the spectrum in the first 40 ns after the start of the pumping pulse and are distributed in a way not reflecting the form of the dispersion spectrum.

At the delay time $\tau = 100$ ns (figure 3*d*), the magnons are spread over the ($k_{||}$, $k_{\perp}$)-plane, mainly occupying states in the proximity of the bottom of the spectrum, but the width of their distribution is still rather large: $\Delta k > 2 \times 10^4\,\mathrm{cm}^{-1}$. Further magnon kinetics can be described as gradual narrowing of the distribution. At the end of this process ($\tau \approx 700$ ns), a very narrow distribution of magnons is formed with a peak centred at the position ($k_{||}^{\min}$, 0) corresponding to f_{min} (figure 3*f*). This is a clear demonstration of the BEC of magnons [9]. We will show below that these magnons demonstrate coherence. It is important to note that as the magnons close to f_{min} are created through a series of multiple scattering events not conserving the phase of individual magnons, the coherence observed in the gas of magnons at the bottom of the spectrum must be a spontaneous one, it cannot be due to the influence of the pumping creating the primary magnons.

The main mechanism responsible for the energy redistribution *within* the magnon system in high-quality epitaxial YIG films is the four-magnon scattering. It is an inelastic scattering mechanism, changing the energies of the participating magnons. As a consequence, it leads to the spreading of the magnons over the spectrum, keeping, however, the number of magnons in the system constant. In parallel, an energy transfer *out* of the magnon system, owing to the spin–lattice (magnon–phonon) interaction, takes place. The influence of the spin–lattice interaction on the magnon kinetics is illustrated by figure 4, which shows the evolution of the magnon population at f_P and f_{min} for a relatively small pumping power $P = 2$ W. In agreement with figure 3, it demonstrates that the density of primary magnons rises very fast and then decreases owing to four-magnon scattering, which redistributes the pumped magnons over the phase space. The dynamics of the magnon population at f_{min} is rather different: it takes about

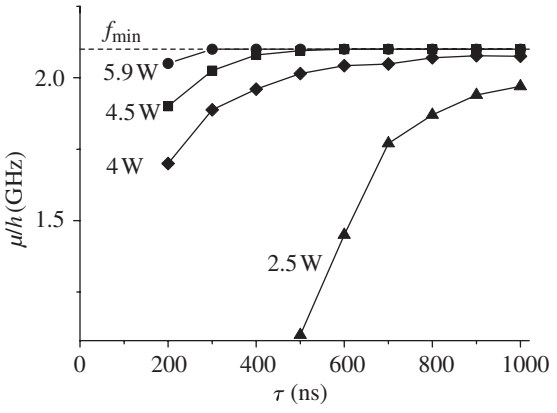

Figure 5. Temporal evolution of the chemical potential of the magnon gas driven by microwave pumping of different powers as indicated. Dashed line indicates the minimum magnon frequency.

200 ns before the density starts to grow, reaching its maximum at $\tau = 550$ ns and then it decreases exponentially. The lifetime $\tau_0 = 260$ ns determined from the exponential part of the curve is due to the energy transfer into the lattice caused by the spin–lattice relaxation.

The four-magnon scattering mechanism redistributing energy within the magnon gas and preserving the number of magnons is much faster than the spin–lattice relaxation [8]. Under this condition, a long pumping pulse creates a gradual wave-like propagation of the population of magnon states starting from the frequency of primary magnons towards the minimum magnon frequency. After a certain transition period characterized by a thermalization time, the magnon gas is characterized by a steady quasi-equilibrium distribution of magnons over the phase space. This steady state corresponds to a thermodynamic state described by the Bose–Einstein statistics. However, contrary to the true equilibrium thermodynamic state, this distribution corresponds to a non-zero chemical potential, which increases with time, as the number of additional magnons injected into the system increases continuously.

Figure 5 illustrates the temporal evolution of the chemical potential for different values of the pumping power. As seen from figure 5, the evolution of the chemical potential strongly depends on the pumping power. For $P > 4.0$ W, the chemical potential reaches its maximum value of $hf_{\min}$ after a certain time delay (300 ns for $P = 5.9$ W), and remains constant up to the end of the pumping pulse, whereas for smaller powers, the chemical potential saturates, not reaching the value $hf_{\min}$. This saturation is due to the flow balance between the excitation of parametric magnons and their slow relaxation caused by the spin–lattice interaction.

4. Bose–Einstein condensation

In pioneering work [4], Einstein described the BEC transition in a gas of weakly interacting particles as follows. Below a critical density of particles N_c, they are distributed over phase space according to the Bose–Einstein statistics. Above the

critical density, the additional particles added to the gas are not distributed over the phase space, but condense at the point corresponding to $f_{\min}$. Let us consider how this scenario is realized in a gas of magnons.

Figure 6 shows the measured BLS spectra under conditions of pumping by long pulses at the different pumping powers $P = 4\,\mathrm{W}$ and 5.9 W. Only data for the delay times corresponding to the quasi-equilibrium distributions of magnons are shown. Filled circles in the figures represent the experimental data, solid lines are the distributions calculated based on Bose–Einstein statistics, using μ as the fit parameter. As seen in figure 6*a*, for $P = 4\,\mathrm{W}$, the chemical potential grows with time and reaches saturation at $\mu/h = 2.08\,\mathrm{GHz}$. This value is close, but still below $f_{\min}$. Apparently, higher values of μ cannot be reached at this pumping power since the pumped magnons leave the magnon gas owing to spin–lattice relaxation. Figure 6*b* illustrates the same process at $P = 5.9\,\mathrm{W}$. For this pumping power, the maximum value $\mu/h = 2.10\,\mathrm{GHz}$ is already reached after 300 ns. One can conclude that the critical density of the magnon gas N_{c} is achieved at $\tau = 300$, and the corresponding distribution can be considered as the critical distribution $n_{\mathrm{c}}(f)$. Further pumping leads to a phenomenon that can be indeed interpreted as BEC of magnons; additionally, pumped magnons are collected at the bottom of the spectrum without changing the population of the states at higher frequencies. The latter fact is also demonstrated by figure 6*b*, showing the high-frequency parts of the magnon distribution curves on an appropriate scale. These data demonstrate that the BLS spectra for $\tau > 300\,\mathrm{ns}$ cannot be described just by increasing the temperature in the Bose–Einstein population function, since a higher temperature means higher magnon populations at *all* frequencies. Thus, figure 6*b* clearly indicates that a Bose–Einstein condensate of magnons is formed.

The issue of the linewidth of the condensate is of great importance for understanding of the degree of coherence of the condensate. From the data presented in figure 6*b*, this linewidth can be estimated as $\Delta f \approx 0.2$–$0.3\,\mathrm{GHz}$. However, this linewidth is defined by the resolution of the spectrometer. Measurements with the higher resolution show that this linewidth is even below 50 MHz. Moreover, microwave spectroscopy indicates that it is narrower than 6 MHz, which corresponds to a very high degree of coherence of magnons in the condensate, giving $\Delta f < 10^{-6} k_{\mathrm{B}} T/h$. Thus, the narrowing of the magnon distribution with respect to that determined by the classical Boltzmann statistics is more than six orders of magnitude!

The detailed theory of BEC of interacting quasi-particles with a finite lifetime is still missing [12–16]. However, one can imagine that, owing to a finite lifetime of the particles, each quantum state is spread in frequency, the width of the spreading δf being determined by the lifetime, τ_0: $\delta f \approx (2\pi\tau_0)^{-1}$. Moreover, a continuous flow of the thermalized magnons, which compensates losses owing to the spin–lattice relaxation, could influence the coherence of the condensate. Therefore, a study of the magnon gas after a short-pumping pulse can provide a clearer insight into spontaneous emergence of coherence in the condensate, which is free from any influence of the external driving force.

The process of magnon relaxation after injection of primary magnons, their thermalization and formation of an overpopulation of the states close to $f_{\min}$ is illustrated in figure 7 [17]. The temporal dependences of the BLS intensity from magnons occupying states close to $f_{\min}$ are shown for different pumping powers,

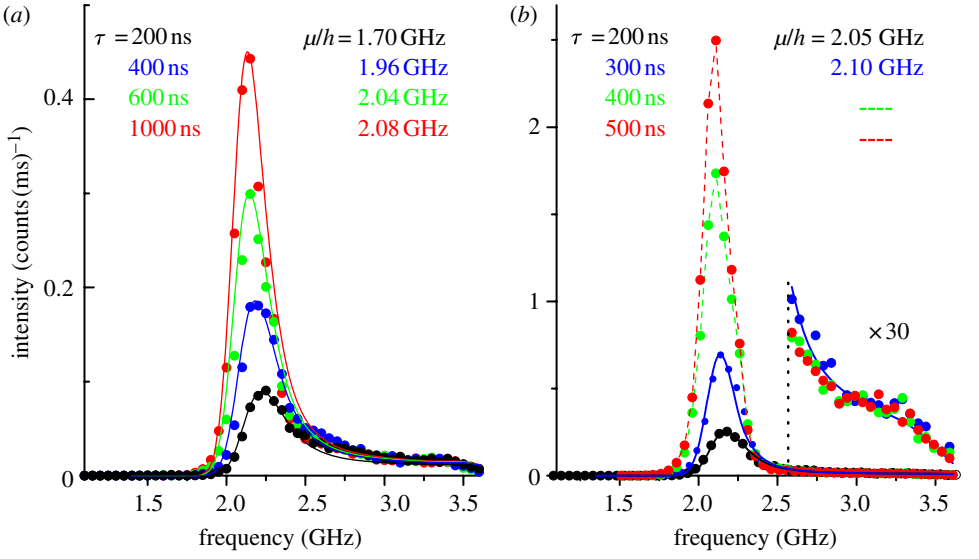

Figure 6. (*a*) BLS spectra from pumped magnons at the pumping power 4 W at different delay times, as indicated. Solid lines show the results of the fit of the spectra based on the Bose–Einstein statistics with the chemical potential being a fit parameter. Note that the critical value of the chemical potential cannot be reached at the used power. (*b*) Same as (*a*) for the pumping power 5.9 W. The critical value of the chemical potential is reached at 300 ns.

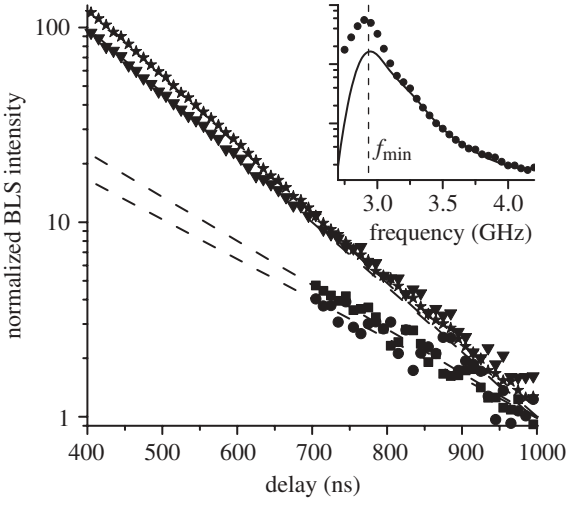

Figure 7. Decay of the BLS intensity at the lowest magnon frequency f_{min} after the formation of the overpopulated state is finished for different values of the pumping power. Lines show the best fit of the experimental points by the exponential decay function. The inset shows the fit of the measured magnon distributions for $P = 6$ W based on Bose–Einstein statistics. Filled circles, $P = 2$ W; filled squares, $P = 2.5$ W; filled inverted triangles, $P = 4$ W; filled stars, $P = 6$ W.

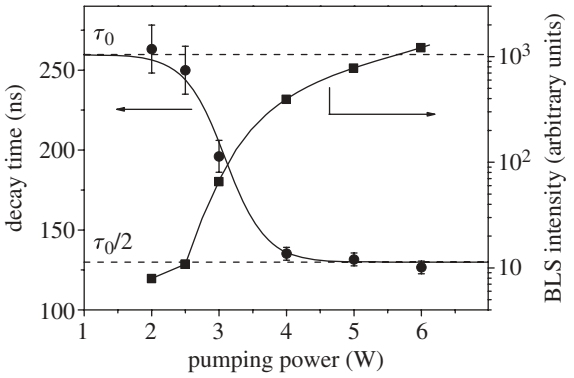

Figure 8. Circles show the measured decay time of the BLS intensity at $f_{\min}$ as a function of the pumping power. Squares show the maximum detected BLS intensity at the frequency $f_{\min}$ versus the pumping power. Corresponding lines are guides for the eye.

corresponding to different numbers of magnons injected during the pumping pulse. The data are shown on a logarithmic scale. Since the absolute value of the scattering intensity strongly depends on the pumping power, the data are normalized at $\tau = 1000$ ns. First, it is seen from the figure that the decay of the BLS intensity at $f_{\min}$ apparently depends on the pumping power. The dashed lines represent the results of the best fit of the experimental points by the exponential decay function. Since the formation of the overpopulated state at $f_{\min}$ happens faster for higher pumping powers, the data for smaller powers start at larger delays.

To understand this finding, one should consider the relation between the BLS intensity and the magnon density in more detail. The BLS intensity is proportional to the temporal average of the square of the electric field of the scattered light, E (e.g. [18]). In the case of many scatterers, the total scattering intensity is proportional to $\langle(\sum E_i)^2\rangle$, where E_i is the scattered field of the ith scatterer. It is obvious that the total scattering intensity of incoherent scatterers is proportional to $\langle\sum E_i^2\rangle$, i.e. to the number of the scatterers, N, owing to zeroing of all cross-correlators of scattered fields: $\langle E_i E_j\rangle = 0$, $i \neq j$. On the contrary, in the case of in-phase coherent scatterers with equal scattering amplitudes, the above cross-correlators are not zero $\langle E_i E_j\rangle = \langle E_i^2\rangle$, and the scattering intensity is proportional to N^2. Thus, comparing the temporal dependence of the BLS intensity and that of the number of scattering magnons, one can detect the magnon coherence. In fact, if the magnon density decays as $n \propto \exp(-\tau/\tau_0)$, the BLS intensity in the case of incoherent magnons should follow the same function. However, for the case of coherent magnons, the BLS intensity should follow $n^2 \sim (\exp(-\tau/\tau_0))^2 = \exp(-2\tau/\tau_0) = \exp(-\tau/(\tau_0/2))$. In other words, for the same decay of the magnon density, the BLS intensity decays twice as fast for coherent magnons than that for incoherent magnons. The experimentally measured decay times of the BLS intensity at $f_{\min}$ as a function of the pumping power P are presented in figure 8. It is clearly seen from figure 8 that the decay time reduces in a stepwise manner by a factor of two with pumping power increasing from 2.5 to 4 W. Based on the above analysis, one has to conclude that

for pumping powers $P \geq 2.5\,\mathrm{W}$, the magnons at $f_{\min}$ start to form a coherent Bose–Einstein condensate and the contribution of the condensate to BLS dominates for $P \geq 4\,\mathrm{W}$. This fact is further corroborated by the inset in figure 7, where the magnon distribution for the maximum pumping power $P = 6\,\mathrm{W}$ and $\tau = 200\,\mathrm{ns}$ is shown together with results of the fit using the Bose–Einstein distribution function. One can see that Bose–Einstein statistics nicely describe the magnon distribution in the entire frequency range, except at the point $f_{\min}$, where a narrow peak (note the logarithmic scale) is created by indicating the existence of a magnon condensate. Thus, our experimental data clearly show that the magnons accumulated at $f_{\min}$ are coherent at high enough pumping powers and this coherence emerges spontaneously if the density of magnons exceeds a certain critical value.

The BEC transition and emergence of coherence in the magnon gas should also lead to an abrupt increase of the BLS intensity at $f_{\min}$, since $N^2 \gg N$. In order to demonstrate this fact, the maximum value of the BLS intensity at $f_{\min}$ versus pumping power P is also plotted in figure 8. One should pay attention to the logarithmic scale for the y-axis and to the fact that experimental error for this curve is smaller than the size of the symbols. As seen from the figure, the dependence demonstrates a clear kink at $P = 2.5\,\mathrm{W}$, marking the onset of the BEC transition.

5. Conclusion

In conclusion, we have investigated the kinetics and thermalization of a magnon gas driven by microwave parametric pumping to a quasi-equilibrium state with a non-zero chemical potential. For a certain critical value of the pumping power, BEC of magnons occurs. For short pumping pulses, this state is free from any influence of the external driving force and is mainly governed by the internal interactions between magnons. We found that starting from a certain critical density, the magnons accumulated at the lowest energy state become coherent. The obtained results are in accordance with the concept of BEC and give undoubted experimental evidence of the existence of a Bose–Einstein condensate at room temperature.

Support by the Deutsche Forschungsgemeinschaft, by the Science and Technology Center of Ukraine, and by the Fundamental Researches State Fund of Ukraine is gratefully acknowledged.

References

1 Bloch, F. 1930 Zur Theorie des Ferromagnetismus. *Z. Phys.* **61**, 206–219. (doi:10.1007/BF01339661)
2 Holstein, T. & Primakoff, H. 1940 Field dependence of the intrinsic domain magnetization of a ferromagnet. *Phys. Rev.* **58**, 1098–1113. (doi:10.1103/PhysRev.58.1098)
3 Dyson, F. J. 1956 General theory of spin–wave interactions. *Phys. Rev.* **102**, 1217–1230. (doi:10.1103/PhysRev.102.1217)
4 Einstein, A. 1925 Quantentheorie des einatomigen idealen Gases. *Sitzungsberg. Ber. Preuss. Akad. Wiss.* **1**, 3–14.
5 Giamarchi, T., Rüegg, Ch. & Tchernyschyov, O. 2008 Bose–Einstein condensation in magnetic insulators. *Nat. Phys.* **4**, 198–204. (doi:10.1038/nphys893)
6 Landau, L. D. & Lifshitz, E. M. 1980 *Statistical physics*. Oxford, UK: Reed Publishing.

7 Snoke, D. 2006 Condensed-matter physics: coherent questions. *Nature* **443**, 403–404. (doi:10.1038/443403a)

8 Demidov, V. E., Dzyapko, O., Demokritov, S. O., Melkov, G. A. & Slavin, A. N. 2007 Thermalization of a parametrically driven magnon gas leading to Bose–Einstein condensation. *Phys. Rev. Lett.* **99**, 037205. (doi:10.1103/PhysRevLett.99.037205)

9 Demidov, V. E., Dzyapko, O., Buchmeier, M., Stockhoff, T., Schmitz, G., Melkov, G. A. & Demokritov, S. O. 2008 Magnon kinetics and Bose–Einstein condensation studied in phase space. *Phys. Rev. Lett.* **101**, 257201. (doi:10.1103/PhysRevLett.101.257201)

10 Demokritov, S. O., Demidov, V. E., Dzyapko, O., Melkov, G. A., Serga, A. A., Hillebrands, B. & Slavin, A. N. 2006 Bose–Einstein condensation of quasi-equilibrium magnons at room temperature under pumping. *Nature* **443**, 430–433. (doi:10.1038/nature05117)

11 Demokritov, S. O., Hillebrands, B. & Slavin, A. N. 2001 Brillouin light scattering studies of confined spin waves: linear and nonlinear confinement. *Phys. Rep.* **348**, 441–489. (doi:10.1016/S0370-1573(00)00116-2)

12 Rezende, S. M. & Zagury, N. 1969 Coherent magnon states. *Phys. Lett. A* **29**, 47–48. (doi:10.1016/0375-9601(69)90788-9)

13 Rezende, S. M. 2009 Theory of microwave superradiance from a Bose–Einstein condensate of magnons. *Phys. Rev. B* **79**, 060410R. (doi:10.1103/PhysRevB.79.060410)

14 Rezende, S. M. 2009 Theory of coherence in Bose–Einstein condensation phenomena in a microwave-driven interacting magnon gas. *Phys. Rev. B* **79**, 174411. (doi:10.1103/PhysRevB.79.174411)

15 Loktev, V. M. 2008 Contribution to the theory of the interaction of electromagnetic radiation with a Bose–Einstein condensate of magnons. *Low Temp. Phys.* **34**, 178–181. (doi:10.1063/1.2887869)

16 Tupizin, I. S., Stamp, P. C. E. & Burin, A. L. 2008 Stability of Bose–Einstein condensates of hot magnons in yttrium iron garnet films. *Phys. Rev. Lett.* **100**, 257202. (doi:10.1103/PhysRevLett.100.257202)

17 Demidov, V. E., Dzyapko, O., Demokritov, S. O., Melkov, G. A. & Slavin, A. N. 2007 Observation of spontaneous coherence in Bose–Einstein condensate of magnons. *Phys. Rev. Lett.* **100**, 047205. (doi:10.1103/PhysRevLett.100.047205)

18 Cottam, M. & Lockwood, D. 1986 *Light scattering in magnetic solids*. New York, NY: Wiley.